Hindawi
Mathematical Problems in Engineering
Volume 2019, Article ID 1083706, 7 pages
https://doi.org/10.1155/2019/1083706

Research Article

Analysis of NMR Spectrometer Receiver Noise Figure

Peter Andris,[1] **Earl F. Emery**,[2] **and Ivan Frollo**[1]

[1]*Institute of Measurement Science, Slovak Academy of Sciences, Dúbravská Cesta 9, 841 04 Bratislava, Slovakia*
[2]*Tecmag, Inc., 10161 Harwin Dr., Suite 150, Houston, TX 77036, USA*

Correspondence should be addressed to Peter Andris; umerandr@savba.sk

Received 13 February 2019; Accepted 16 May 2019; Published 26 June 2019

Academic Editor: Giorgio Besagni

This article describes the measurement and evaluation of the system noise figure of a nuclear magnetic resonance spectrometer. A method was used which involved the console of the spectrometer, calibrated for real voltage (in volts), and used for noise signal digitisation and measurement. The resulting digitised signal was exported and processed, and the root mean square value calculated. This value was utilised for the noise power calculation, which was compared with the theoretical value and the noise figure calculated. The method presented enables analysis of the bandwidth of the noise. Many of the equations that are commonly used for signal processing have been derived for the specific task and require verification. We have verified the technique using a commercial console with two preamplifier pairs. The experimental data agree well with the theoretical values, confirming that the presented method is a valid, simple, and fast tool for the inspection of the spectrometer receiver.

1. Introduction

Many parameters of complex instrumentation must be checked regularly in order to ensure that high quality results are reported. The noise figure is an important parameter of the receiver in a nuclear magnetic resonance (NMR) spectrometer. Regular inspection of the receiver can reveal defects of the hardware or sources of interference. It is possible to measure the noise voltage only, but the noise figure is a widely reported parameter, and so use of this value allows for easy comparison. Professional instruments for noise figure measurement are expensive and only provide accurate results for frequencies above tens of MHz. At frequencies of MHz, the noise figure must be measured using different instruments such as the console of the NMR instrument [1]. The noise figure can be calculated by processing the measured noise voltage; however, some researchers have calculated the noise figure from continuous signals rather than discrete signals [2–4]. The noise level is always evaluated as part of a basic NMR experiment [5, 6]. Connecting the receiver coils of the NMR using inductive coupling can provide some advantages [7, 8] (higher comfort for operators, balancing the receive coil), and the noise figure of the entire inductively coupled system can be calculated using an equation [7]. Signal processing and noise matching have been used to optimise NMR results [9–15], although optimisation must be carried out in a manner specific to the particular experiment.

The system noise figure at frequencies of MHz can be determined using the "hot/cold resistor" method; however, this method has the disadvantage of requiring liquid nitrogen to cool the cold resistor. Not every working place may be equipped for such operations. The technique that we present here for noise figure determination utilises the NMR console, but in this case it is calibrated to the real values of voltage, and the noise voltage is measured and subsequently processed. Our technique provides a fast and accurate approach which only requires standard laboratory instruments and materials. The measured data is processed in two ways and the results are compared. First the noise figure has been determined at a narrow noise bandwidth, where the spectra may be considered constant and second at wider noise bandwidth with nonconstant spectra using the calculation of the equivalent noise bandwidth. The processing of the measured data is discussed elsewhere [16]. The theory and results described in the present article are useful for technical and experimental purposes and provide a platform for theoretical studies. Moreover, our research offers options for techniques which utilise the NMR spectroscopic console, which is available at

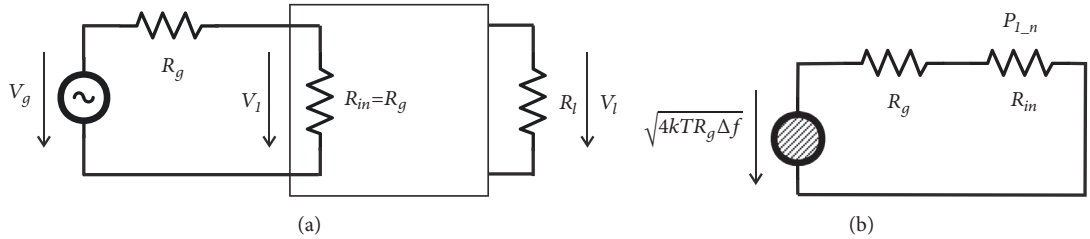

Figure 1: A simplified circuit diagram of the NMR receiver. (a) Signal and noise voltages at the two-port, (b) incoming noise power at the two-port. V_1: group of incoming signal or noise voltages, e.g., V_{1_s}, V_{1_n}, $V_{1\_s\_rms}$, or $V_{1\_n\_mean}$. V_l: group of outgoing signal or noise voltages, e.g., V_{l_s}, V_{l_n}, $V_{l\_s\_rms}$, or $V_{l\_n\_i}$ (i-th term of the samples series). Δf is the noise bandwidth of the receiver. The noise spectra within the noise bandwidth should be constant. V_g is signal voltage from source. R_g, R_{in}, R_l are resistances of source, input resistance of the two-port, and load resistance of the two-port. T is the absolute temperature of the resistance R_g. $\sqrt{4kTR_g\Delta f}$ is RMS value of the thermal noise voltage generated in the resistance R_g (Nyquist equation). P_{1_n} is the noise power from R_g incoming into the two-port.

many NMR laboratories. The technique has been tested at the hardware for measurements at low magnetic field but there is no reason why it could not be used also for higher spectra frequencies.

2. Theory and Methods

A simplified circuit diagram of the receiver is presented in Figure 1(a). All impedances and voltages indicated are real values (not complex). In practice, these values are rarely accurate, but considerable research is dedicated to achieving accuracy, including the application of transmission lines matching.

The power gain of the receiver including the preamplifier can be calculated using (1).

$$G = \frac{V_{l\_s}^2}{V_{1\_s}^2} \bullet \frac{R_{in}}{R_l} \tag{1}$$

Consider the spectra frequencies and impedance temperatures where $hf/kT \ll 1$ ($h = 6.62 \times 10^{-34}$ J/s is the Planck constant; $k = 1.38 \times 10^{-23}$ J/K is the Boltzmann constant). The condition limits the region where the noise is approximated by the Nyquist equation sufficiently accurately. The signal-to-noise ratio (SNR) of the signal incoming into the input of the two-port is given by (2).

$$SNR_1 = \frac{P_{1\_s}}{P_{1\_n}} = \frac{V_{1\_s\_rms}^2/R_{in}}{kT\Delta f} \tag{2}$$

The calculation behind the relationship $P_{1\_n} = kT\Delta f$ [2–4] can be explained using Figure 1(b). The power of the thermal noise P_{1_n}, coming into the receiver from the source impedance R_g, is split into two equal resistances, R_g and R_{in}, and is defined by (3).

$$\begin{aligned} P_{1\_n} &= \frac{R_{in}}{R_g + R_{in}} \bullet \frac{\left(\sqrt{4kTR_g\Delta f}\right)^2}{R_g + R_{in}} \\ &= \frac{1}{2} \bullet \frac{\left(\sqrt{4kTR_g\Delta f}\right)^2}{2R_g} = kT\Delta f \end{aligned} \tag{3}$$

T is the absolute temperature of both R_{in} and the matched source resistance R_{g}, and Δf is the noise bandwidth of the circuit. For impedance matching, $R_g = R_{in}$, the value of P_{1_n} from the noise source (R_{g}) into the input resistance (R_{in}) is maximal and equal to the value of $kT\Delta f$. The SNR of the outgoing signal is given by (4).

$$SNR_l = \frac{P_{l\_s}}{P_{l\_n}} = \frac{V_{l\_s\_rms}^2/R_l}{V_{l\_n\_rms}^2/R_l} = \frac{V_{l\_s\_rms}^2}{V_{l\_n\_rms}^2} \tag{4}$$

Calculation of the noise factor using the incoming and outgoing signal SNRs can be achieved using (5).

$$\begin{aligned} F = \frac{SNR_1}{SNR_l} &= \frac{V_{1\_s\_rms}^2 \bullet V_{l\_n\_rms}^2}{V_{l\_s\_rms}^2 \bullet R_{in}kT\Delta f} = \frac{P_{l\_n}}{G \bullet kT\Delta f} \\ &= K^2 \bullet \frac{V_{l\_n\_rms}^2}{R_{in}kT\Delta f} \end{aligned} \tag{5}$$

Here always $F > 1$. The noise figure in decibels is given by (6).

$$NF = 10 \bullet \log F \tag{6}$$

In practice, the noise factor and the noise figure should be measured at the room temperature $T = T_0 = 290K$.

Calibration of the receiver is carried out using the coefficient K (7).

$$K = \frac{V_{1\_s}}{V_{l\_s}} \tag{7}$$

The coefficient can be measured and calculated using a harmonic signal voltage (RMS, mean or amplitude) from an external signal generator, or using the signal from the transceiver of the console provided that signal measurement is accurate. If K is in volts/ADC units, the receiver is calibrated and F is dimensionless as it should be. The size of V_{1_s} must not exceed the limit for the V_{l_s} truncation. The noise bandwidth of the receiver is not equivalent to the frequency bandwidth of the receiver. The spectrum related to the noise bandwidth should be constant and can be calculated

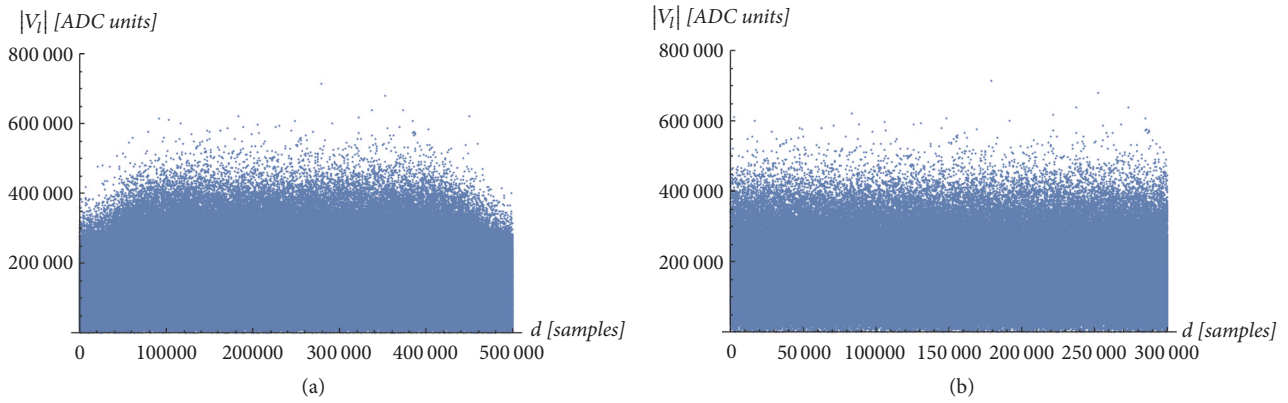

Figure 2: The noise voltage from the matched receiver. (a) All measured modules of frequency samples, (b) cropped frequency samples series. The new series can be used for the noise bandwidth calculation as the spectra are approximately constant.

from the frequency bandwidth (equivalent noise bandwidth), provided that the parameters of the receiver filter are known (gain versus frequency).

Given the shape of the noise spectrum, we present a simplified approach to the calculation. The measured noise voltage output of the matched receiver is shown in Figure 2(a). By cropping both margins of the spectra, we generated modified spectra with a rectangular-shaped noise bandwidth indicating a more constant value of the spectra (Figure 2(b)). This processing should be acceptable for most measurements. Equation (5) requires the route mean square (RMS) value of the output voltage. In order to calculate the RMS voltage, frequency samples must be calculated. By measuring the noise of the matched receiver, we obtained a series of N time domain samples. To convert these into frequency spectra, a discrete Fourier transform (FT) was carried out. The FT can be performed directly using the console or later using computer processing of the exported data. The RMS voltage can then be calculated from the frequency samples ($V_{l\_n\_i}$) using (8). Spectra in Figure 2 consist of absolute values of such frequency samples.

$$V_{\text{l\_n\_rms}} = \sqrt{\frac{1}{N^2}\sum_{i=1}^{N}\left|V_{l\_n\_i}\right|^2} = \sqrt{\sum_{i=1}^{N}\left|\frac{V_{l\_n\_i}}{N}\right|^2} \tag{8}$$

Equation (8) was derived from definition of RMS for time samples using the information in [17] (the Parseval theorem). $V_{l\_n\_i}$ is i-th term of the outgoing noise frequency samples series.

A computer simulation was used for the verification. A time function with known RMS value was selected and given by (9).

$$V_i = A_1 \bullet \cos 2\pi f_1 \Delta t\,(i-1) + A_2 \bullet \cos 2\pi f_2 \Delta t\,(i-1) + A_3 \bullet \cos 2\pi f_3 \Delta t\,(i-1) \tag{9}$$

For $i = 1 \div N$ a vector of time samples was calculated under the following conditions:

number of samples N=10,000

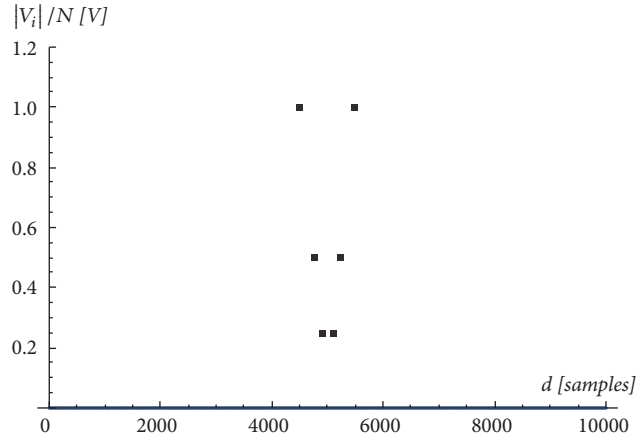

Figure 3: RMS voltages of the spectral components in the verification computer simulation.

frequency $f_1 = 100$ Hz
frequency $f_2 = 250$ Hz
frequency $f_3 = 500$ Hz
time interval $\Delta t = 10^{-4}$ s
amplitude $A_1 = 0.5$ V
amplitude $A_2 = 1.0$ V
amplitude $A_3 = 2.0$ V

The vector was processed using the discrete Fourier transform, resulting in N frequency samples (10).

$$V = V_1 \div V_N \tag{10}$$

At the first sight (8) is similar to an average, but Figure 3 depicts absolute value of spectra (10) divided by N. As assumed, all terms except those corresponding to the harmonic voltages are of zero values. The RMS voltage according to (8) is given by

$$V_{rms} = 1.62019 \text{ V}. \tag{11}$$

Calculate the V_{rms} only for nonzero terms according to Figure 3. It is a known fact that a resulting RMS voltage must be calculated using the quadrates sum of the participating RMS components.

$$V_{rms} = \sqrt{1.0^2 + 0.5^2 + 0.25^2 + 0.25^2 + 0.5^2 + 1.0^2} = 1.62019 \text{ V} \quad (12)$$

A transform to single sided spectrum yields

$$V_{rms} = \sqrt{\frac{0.5^2}{2} + \frac{1.0^2}{2} + \frac{2.0^2}{2}} = 1.62019 \text{ V}. \quad (13)$$

It indicates the following.

$$V_{1\_rms} = \frac{A_1}{\sqrt{2}}$$
$$V_{2\_rms} = \frac{A_2}{\sqrt{2}} \quad (14)$$
$$V_{3\_rms} = \frac{A_3}{\sqrt{2}}$$

This are generally known RMS values of a real (not complex) harmonic signal.

It is evident that the RMS voltage of the i-th frequency sample is given by (15).

$$V_{i\_rms} = \frac{|V_i|}{N} \quad (15)$$

The RMS voltage of all N samples is given by (8).

For cropping of noise bandwidth, (8) can be modified to

$$V_{\text{l\_n\_rms}} = \sqrt{\left(\frac{1}{N}\right)^2 \bullet \sum_{i=n_1}^{n_2} |V_{l\_n\_i}|^2} \quad (16)$$

where $1 \le n_1 < n_2 \le N$.

Ultimately, the first noise factor is calculated using

$$F_1 = K^2 \frac{\left(1/N^2\right) \sum_{i=1}^{d} |V_{l\_n\_i}|^2}{kT\left((d-1)/NT_s\right) R_{in}} \quad (17)$$

where d is the number of samples after cropping and T_s is the sampling time interval of the samples.

For verification, we compared results using our simplified approach with those obtained using the conventional calculation (equivalent noise bandwidth), with (16)-(17) described previously. The noise spectra in Figure 2(a) are the white noise created by resistance matching of the receiver input including a preamplifier, amplified by the receiver. Thus, the spectral envelope is modulated by the gain of the receiver and the receiver filter. The equivalent number of samples is given by (18).

$$dd = \frac{\sum_{i=1}^{N} |V_{l\_n\_i}|^2}{\overline{\left|V_{l\_n\_i}^2\right|}(f_0)} \quad (18)$$

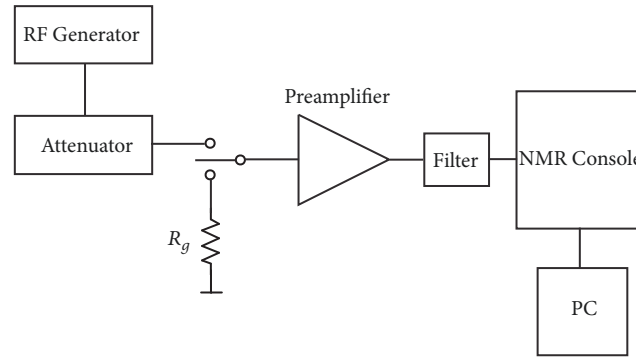

Figure 4: Block diagram of the verification experiment.

The second powers of all sample voltages are summed and divided by the mean value of $|V_{l\_n\_i}|^2$ round the operation frequency f_0. The second noise factor for the entire frequency bandwidth of the receiver is given by (19).

$$F_2 = K^2 \frac{\left(1/N^2\right) \sum_{i=1}^{N} |V_{l\_n\_i}|^2}{kT\left((dd-1)/NT_s\right) R_{in}} \quad (19)$$

Sample noise can be eliminated in two ways: by filtering the measured voltages of samples using a software low-pass filter or by averaging the noisy samples. Following the latter option, we calculated $\overline{|V_{l\_n\_i}^2|}(f_0)$ of 10,000 frequency samples and compared the results of both approaches (17) and (19) for noise factors calculation. The values of F_1 and F_2 (NF_1 and NF_2) should be similar but do not have to be equal.

The measured noise signal was compared to the theoretical values of the noise power, which ensures excellent comparability with other systems.

The processed data have been measured under the following conditions:

operation frequency of the scanner: f_0=4.45 MHz

sampling interval: T_s = 100 μs

frequency bandwidth of the receiver: B = 10 kHz

temperature of R_g: T=290 K

original number of samples: N=500,000

number of samples after cropping: d=300,000

Verification experiments were performed in Bratislava and Houston on similar but not the same instrumentation. Therefore only the results measured in Bratislava are published in this article. Nevertheless, the results from Houston were important for verification of the experimental results, carried out in Bratislava, mainly in the beginning of the work.

Block diagram of the verification experiment is depicted in Figure 4. An external RF generator is assumed for the receiver calibration.

3. Results

Verification experiments were performed on an experimental NMR scanner equipped with a home-made resistive magnet of 0.1 T and the Apollo spectroscopic NMR console

Table 1: Results of verification.

No.	f_0[MHz]	Preamplifier; NF	NF_1[dB]	NF_2[dB]	Filter	d[samples]	N[samples]
1	4.45	broadband-1; 1 dB	4.4	4.42	No	300,000	500,000
2	4.45	broadband-2; 1 dB	4.45	4.42	No	300,000	500,000
3	4.45	broadband-1; 1 dB	1.45	1.37	L-P	300,000	500,000
4	4.45	broadband-2; 1 dB	1.48	1.51	L-P	300,000	500,000
5	4.45	tuned-1; 1 dB	1.34	1.27	No	300,000	500,000
6	4.45	tuned-2; 1 dB	1.53	1.66	No	300,000	500,000
7	4.45	tuned-1; 1 dB	1.36	1.29	L-P	300,000	500,000
8	4.45	tuned-2; 1 dB	1.44	1.48	L-P	300,000	500,000

(Tecmag Inc., Houston, TX). The console was utilised for imaging, operated at a frequency of 4.45 MHz. Console calibration was performed using the GFG-3015 function generator (Good Will Instrument Co., Ltd., New Taipei City, Taiwan). Calibration using the console transceiver was also tested in Houston. An external attenuator was necessary in both cases. The broadband preamplifier pair of AU-1579 (MITEQ, Hauppauge, NY) with 50-Ohm input and output impedances and $NF = 1$ dB (a catalogue datum) was used (selected randomly from three pieces). Another tuned preamplifier pair P4.45VD (Advanced Receiver Research, Burlington, CT) with 50-Ohm input and output impedances and $NF = 1$ dB (a catalogue datum) was also used, selected randomly from three pieces. We verified our theory through several experiments, the results of which are presented in Table 1. The receiver with MITEQ broadband preamplifiers exhibited significant noise, which was improved by inserting a low-pass filter between the preamplifier and the console. The low-pass filter applied had a cut-off frequency of 10.7 MHz: SLP-10.7+ (Mini-Circuits, Brooklyn, NY). Using a filter with a cut-off frequency closer to the operation frequency of the spectrometer may further improve the noise figure value; however, the noise figure obtained with broadband preamplifiers and filters is similar to that observed using tuned preamplifiers. The data obtained using tuned ARR preamplifiers did not require a filter as the measured noise figure values were in good agreement with the catalogue data. Only small differences were seen between the results of d (cropped) samples compared with those from N samples. The difference did not exceed 0.13 dB (experiment no. 6, tuned-2 without a filter). All measurements were performed in the shielding cage of the scanner, and all connections used shielded cables. Measurements without a shielding cage resulted in much higher noise, which varied between measurements depending on the actual interference in the measurement space. Shielded cables alone are therefore not sufficient for an accurate measurement, and all instruments should be warmed up for some time before measurements are carried out. Also, changes in the inputs and outputs of the preamplifiers should be performed some time before the measurement.

The noise figures of the receiver with each of the four preamplifiers depending on the noise bandwidth are shown in Figure 5. It can be seen that for frequencies close to f_0, the measured noise figure is inaccurate, possibly due to the low number of frequency samples. Between 50,000 and 300,000 samples, the value is approximately constant, falling rapidly beyond 300,000 samples.

The frequency, or noise bandwidth, in Hz can be estimated using (20), taken from the graph of Figure 6.

$$B = \frac{d}{NT_s} \tag{20}$$

The results of the noise figure measurements reflect our expectations, and it can therefore be concluded that the verification was successful. Furthermore, equations and derived formulae provided acceptable results.

4. Discussion and Conclusions

The purpose of this study was to develop and to test a technique for the determination of the NMR spectrometer receiver noise figure. We endeavoured to use only widely available or cheap instruments. The noise figure of the receiver obtained using a broadband preamplifier depends on the filter between the preamplifier and the console. The filter type and characteristic frequencies are the subject of further studies. It is possible that a suitable selection of frequencies could improve the noise figure of the entire receiver, which cannot be achieved by replacing the hardware low-pass filter with a suitable software low-pass filter. This suggests that the point of the receiver chain at which the filter is connected is an important consideration. Measured data was processed using calculations from the cited sources, but also from own derivations. The final results have proven that all the equations and derived formulae are correct. In the present study, methods were tested using a spectroscopic NMR console. However, the console must be able to calibrate the voltage in order to carry out the calculations, and so this may not be possible on all consoles.

The primary application of the technique is to inspect the receiver of the spectrometer, but in some cases it can be applied for analysis of the noise figure of a tested preamplifier measurement. The method can be also applied to a magnetic resonance imaging (MRI) scanner, provided that the console is suitable. If the signal for the console is amplified by a broadband preamplifier, it is recommended that a suitable filter is connected between the preamplifier and the console for significant improvements in the noise figure.

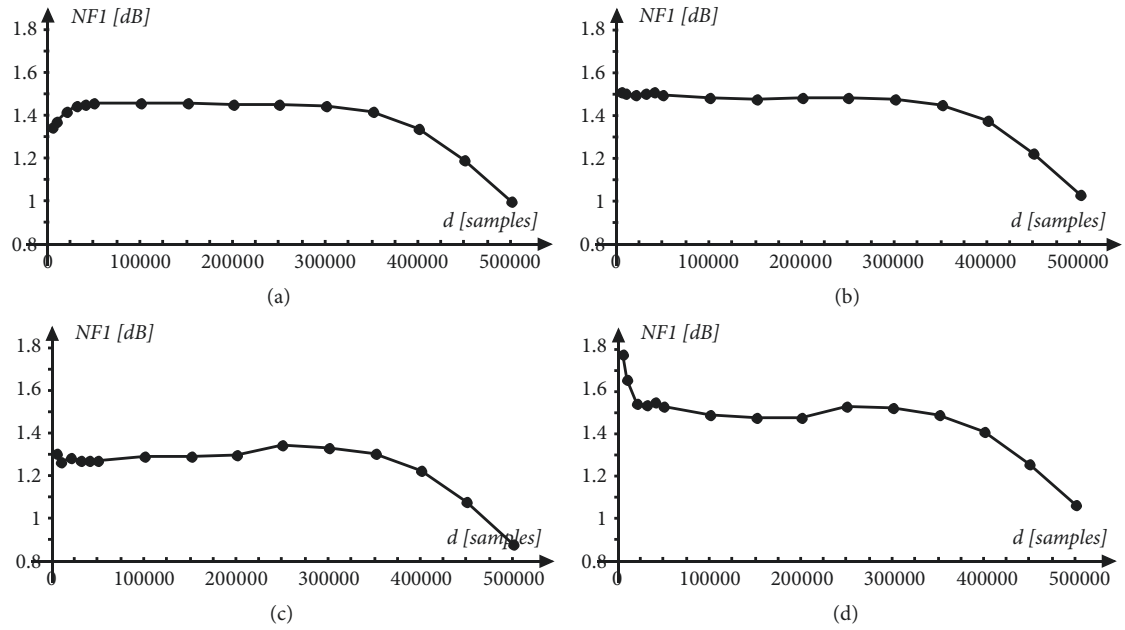

Figure 5: Influence of the noise bandwidth on the measured receiver noise figure using (a) the broadband-1 preamplifier, (b) the broadband-2 preamplifier, (c) the tuned-1 preamplifier, and (d) the tuned-2 preamplifier. The noise bandwidth d is symmetrical to the operation frequency f_0.

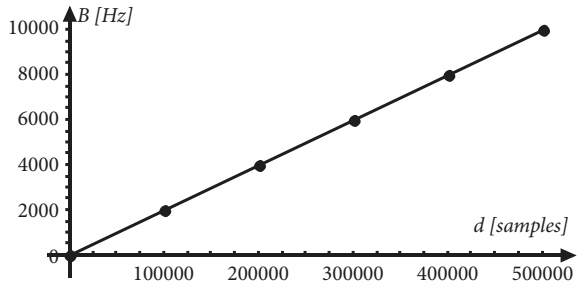

Figure 6: Calculation of the noise or frequency bandwidth (B) from frequency samples.

Data Availability

The measured digital data used to support the findings of this study are available from the corresponding author upon request.

Conflicts of Interest

The authors declare that there are no conflicts of interest regarding the publication of this paper.

Acknowledgments

This work was supported by the Scientific Grant Agency VEGA 2/0001/17 and within the project of the Research and Development Agency No. APVV-15-0029.

References

[1] P. Andris, V. Jacko, T. Dermek, and I. Frollo, "Noise measurement of a preamplifier with high input impedance using an NMR console," *Measurement*, vol. 55, pp. 408–412, 2014.

[2] V. Žalud and V. N. Kulešov, *Semiconductor Circuits with Low Noise*, SNTL, Prague, Czechia, 1980 (in Czech).

[3] H. Bittel and L. Storm, *Noises*, Springer-Verlag, Berlin, Germany, 1971 (in German).

[4] B. Schiek and H. J. Siweris, *Noises in RF Circuits*, Hüthig, Heidelberg, Germany, 1990 (in German).

[5] D. Hoult and R. Richards, "The signal-to-noise ratio of the nuclear magnetic resonance experiment," *Journal of Magnetic Resonance*, vol. 24, no. 1, pp. 71–85, 1976.

[6] D. Hoult and P. C. Lauterbur, "The sensitivity of the zeugmatographic experiment involving human samples," *Journal of Magnetic Resonance*, vol. 34, no. 2, pp. 425–433, 1979.

[7] A. Raad and L. Darrasse, "Optimization of NMR receiver bandwidth by inductive coupling," *Magnetic Resonance Imaging*, vol. 10, no. 1, pp. 55–65, 1992.

[8] M. Decorps, P. Blondet, H. Reutenauer, J. Albrand, and C. Remy, "An inductively coupled, series-tuned NMR probe," *Journal of Magnetic Resonance*, vol. 65, no. 1, pp. 100–109, 1985.

[9] J. Weis, A. Ericsson, and A. Hemmingsson, "Chemical shift artifact-free microscopy: spectroscopic microimaging of the human skin," *Magnetic Resonance in Medicine*, vol. 41, no. 5, pp. 904–908, 1999.

[10] P. Marcon, K. Bartusek, Z. Dokoupil, and E. Gescheidtova, "Diffusion MRI: mitigation of magnetic field inhomogeneities," *Measurement Science Review*, vol. 12, no. 5, pp. 205–212, 2012.

[11] K. Bartusek, Z. Dokoupil, and E. Gescheidtova, "Mapping of magnetic field around small coils using the magnetic resonance method," *Measurement Science and Technology*, vol. 18, no. 7, pp. 2223–2230, 2007.

[12] D. Nespor, K. Bartusek, and Z. Dokoupil, "Comparing Saddle, Slotted-tube and Parallel-plate Coils for Magnetic Resonance Imaging," *Measurement Science Review*, vol. 14, no. 3, pp. 171–176, 2014.

[13] P. Latta, M. L. Gruwel, V. Volotovskyy, M. H. Weber, and B. Tomanek, "Simple phase method for measurement of magnetic field gradient waveforms," *Magnetic Resonance Imaging*, vol. 25, no. 9, pp. 1272–1276, 2007.

[14] P. Latta, M. L. Gruwel, V. Volotovskyy, M. H. Weber, and B. Tomanek, "Single-point imaging with a variable phase encoding interval," *Magnetic Resonance Imaging*, vol. 26, no. 1, pp. 109–116, 2008.

[15] D. Gogola, P. Szomolanyi, M. Škrátek, and I. Frollo, "Design and construction of novel instrumentation for low-field MR tomography," *Measurement Science Review*, vol. 18, no. 3, pp. 107–112, 2018.

[16] G. Wimmer, V. Witkovský, and T. Duby, "Proper rounding of the measurement results under normality assumptions," *Measurement Science and Technology*, vol. 11, no. 12, pp. 1659–1665, 2000.

[17] D. W. Kammler, *A First Course in Fourier Analysis*, Cambridge University Press, New York, NY, USA, 2007.